ROYAL SOCIETY OPEN SCIENCE

royalsocietypublishing.org/journal/rsos

Research

Cite this article: Booth DJ, Griffiths I, Howell P. 2026 Dipole and pairwise models for the motion of bubbles in a Hele-Shaw cell. *R. Soc. Open Sci.* **13**: 252426.
https://doi.org/10.1098/rsos.252426

Received: 9 December 2025
Accepted: 17 December 2025

Subject Category:
Mathematics

Subject Areas:
applied mathematics, fluid mechanics

Keywords:
Hele-Shaw, bubbles, microfluidics, asymptotics, thin films, complex potential

Authors for correspondence:
Daniel J. Booth
e-mail: daniel.j.booth@warwick.ac.uk
Ian Griffiths
e-mail: Ian.Griffiths@maths.ox.ac.uk
Peter Howell
e-mail: Howell@maths.ox.ac.uk

Supplementary material is available online at https://doi.org/10.6084/m9.figshare.c.8311165.

THE ROYAL SOCIETY PUBLISHING

Dipole and pairwise models for the motion of bubbles in a Hele-Shaw cell

Daniel J. Booth[1,2], Ian Griffiths[1] and Peter Howell[1]

[1]Mathematical Institute, University of Oxford, Oxford, UK
[2]Department of Mathematics, University of Warwick, Coventry, UK

DJB, 0000-0001-6166-0801; IG, 0000-0001-6882-7977

We consider the motion of an arbitrary number of approximately circular bubbles in a Hele-Shaw cell. Each bubble is assumed to be large enough that it is flattened by the cell walls into a pancake-like shape, but small enough to remain approximately circular in plan view. Numerical solutions of the full Hele-Shaw problem become computationally expensive when there is a large number of bubbles. It is therefore common in the literature when modelling a large number of bubbles to assume that each bubble acts like a dipole. Here, we provide the theoretical basis for this approach through the use of matched asymptotic expansions, in the limit where the bubbles are all far apart. We find that this method qualitatively reproduces the behaviour of the full model at a much-reduced computational cost, provided the bubbles remain well separated. We also derive a pairwise interaction model by summing over the contributions owing to each possible bubble pair. This improved model has computational complexity comparable to that of the dipole model but remains valid in situations in which two bubbles become close.

1. Introduction

The dynamics of bubbles in a Hele-Shaw cell is both a classical fluid dynamics problem [1–4] and a fundamental mathematical problem owing to its connection to potential theory and complex analysis [5–9]. Microfluidic devices often involve the transport of many bubbles along a Hele-Shaw channel [10–13]. In such devices, the bubbles are often large enough that they are flattened into pancake-like shapes [14,15], with thin liquid films separating the bubbles from the walls, but also small enough to remain approximately circular in plan view [16].

Booth *et al.* [17] derived a general model for the motion of such bubbles in a Hele-Shaw cell incorporating the additional pressure drop found by Bretherton [18] across each bubble meniscus owing to the thin films. The model for a single bubble was

experimentally validated by Wu *et al.* [16], while systems involving pairs of bubbles were analysed both theoretically and experimentally by Booth *et al.* [19]. Booth *et al.* [17] found that, in systems of three or more identical collinear bubbles, the middle bubbles travel either faster or slower than the outer two depending on the flow conditions, resulting in 'Newton's cradle'-like behaviour. However, the model of Booth *et al.* [17] becomes unwieldy when considering the motion of a large number of bubbles, a situation that is common in bubble-laden microfluidic devices. Reduced-order models are therefore attractive to allow for fast and accurate simulation of many-bubble systems.

It is common in the literature, when modelling a large number of bubbles, to assume without rigorous justification that each bubble acts like a dipole [20–22]. Green [23] showed that the two-bubble solution of Sarig *et al.* [24] reduces to a dipole interaction in the limit where the bubbles are far apart, before generalizing this result to an arbitrary number of bubbles in a non-rigorous manner. Pumir & Aref [25] derived a dipole model for the motion of bubbles in a stagnant outer fluid by taking the leading-order contribution to the Green's function representation of the fluid velocity; however, they did not account for the drag owing to the thin films between the bubbles and the cell walls. Often, the dipole model is supplemented by an ad hoc drag law to account for the friction owing to these thin films above and below the bubble [20,23]. Such models include a free parameter that needs to be fitted with experimental data. Here, we use matched asymptotic expansions to analyse the full Hele-Shaw model, incorporating the Bretherton drag [18], thus accurately modelling the effect of the thin films and resulting in a dipole model with no free parameters. We further improve upon the dipole approach by deriving a pairwise interaction model that can accurately capture situations in which two bubbles become close and the dipole model breaks down.

The paper is structured as follows. In §2, we write down the governing equations for the motion of an arbitrary number of bubbles in a Hele-Shaw cell. In §3, we derive a dipole model, in which the bubbles are assumed to be well separated and therefore interact like dipoles. Then, in §4, we derive an alternative pairwise interaction model by summing over the contributions from each bubble pair. In §5, we compare the predictions of the two simplified models with each other and with numerical solutions of the full problem. Finally, in §6, we summarize our key findings.

2. General model for multiple bubbles

We begin by summarizing the model derived in Booth *et al.* [17] to describe the flow of an arbitrary number of bubbles in a Hele-Shaw cell of height $\hat{h}$. Here, $\hat{h}$ is assumed to be much smaller than the horizontal dimensions of the cell, so we can employ lubrication theory. Each bubble is flattened by the cell walls above and below, causing it to have a pancake-like shape and an approximately circular profile when viewed from above (figure 1). Each bubble's radius is denoted by $\hat{R}_k \gg \hat{h}$ for $1 \leq k \leq N$, where N is the total number of bubbles. We prescribe a uniform unidirectional flow with velocity $\hat{\boldsymbol{U}}$ in the far field. The viscosity of the liquid and the liquid–air surface tension are denoted by $\hat{\mu}$ and $\hat{\gamma}$, respectively. Finally, we assume that the side walls of the cell are sufficiently far away from the bubbles that we can treat the Hele-Shaw cell as having an infinite extent.

We non-dimensionalize the system by scaling lengths with a typical bubble radius $\hat{R}$, velocities with $|\hat{\boldsymbol{U}}|$ and the fluid pressure with $12\hat{\mu}|\hat{\boldsymbol{U}}|\hat{R}/\hat{h}^2$. The dimensionless depth-averaged fluid velocity $\boldsymbol{u}$ and pressure p are then related by $\boldsymbol{u} = -\boldsymbol{\nabla} p$; for a full derivation of the Hele-Shaw model see [26]. We construct a dimensionless Cartesian coordinate system (x, y) in the plane of the cell, with the x-axis parallel to the imposed uniform flow. We thus obtain the following dimensionless model, in which dimensionless variables are denoted without hats:

$$\nabla^2 p = 0 \quad \text{in} \quad \Omega \qquad \text{(incompressibility)}, \tag{2.1a}$$

$$\boldsymbol{n} \cdot \boldsymbol{\nabla} p = -\boldsymbol{U}_k \cdot \boldsymbol{n} \quad \text{on} \quad \partial\Omega_k \qquad \text{(kinematic boundary condition)}, \tag{2.1b}$$

$$p \sim -x \quad \text{as} \quad x^2 + y^2 \to \infty \qquad \text{(far-field uniform flow)}, \tag{2.1c}$$

where Ω is the fluid domain, while $\partial\Omega_k$ and $\boldsymbol{U}_k = (U_k, V_k)$ are the boundary and the *a priori* unknown velocity of the kth bubble, respectively. We note that in equation (2.1b) we have neglected the contribution owing to leakage through the thin films, because the effect is always subdominant and only offers a correction of the order $\mathrm{Ca}^{2/3}$ [16,27,28]. We illustrate the solution domain schematically in figure 1 for an example with three bubbles.

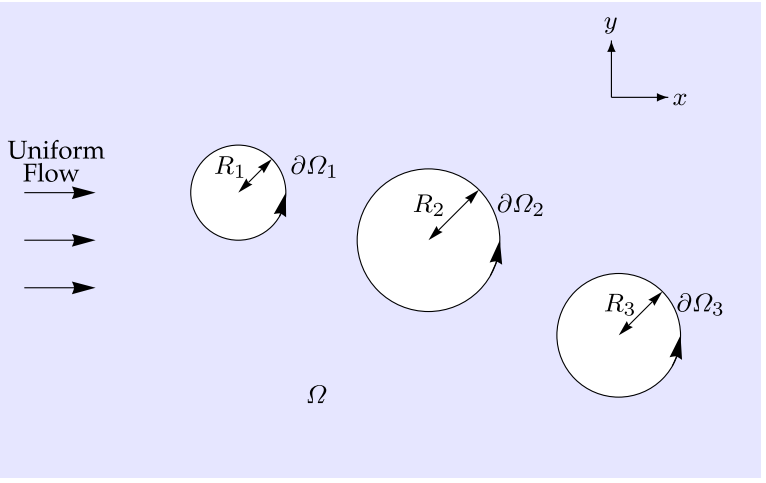

Figure 1. Schematic plan view for the flow of three bubbles. The kth bubble has dimensionless radius R_k.

There are two dimensionless parameters associated with our problem, namely the aspect ratio and the capillary number, defined by

$$\epsilon = \frac{\hat{h}}{2\hat{R}}, \qquad \mathrm{Ca} = \frac{\hat{\mu}\hat{U}}{\hat{\gamma}}, \tag{2.2}$$

respectively, both of which are assumed to be small. Specifically, in the distinguished limit where $\mathrm{Ca} = O(\epsilon^3)$ as $\epsilon \to 0$, both bubbles remain circular to leading order, and p is therefore fully determined by the problem equations (2.1) (up to an irrelevant constant) once the bubble velocities $\boldsymbol{U}_k$ are all specified. To close the system, we follow Booth *et al.* [17] and perform an effective net force balance on each bubble to obtain

$$\frac{\boldsymbol{U}_k}{|\boldsymbol{U}_k|^{1/3}} = \frac{\delta}{\pi R_k} \oint_{\partial\Omega_k} -p\boldsymbol{n}\,\mathrm{d}s, \tag{2.3}$$

where R_k is the dimensionless radius of the kth bubble. Here, δ denotes the *Bretherton parameter* [17], defined by

$$\delta = \frac{1}{\eta}\frac{\mathrm{Ca}^{1/3}}{\epsilon} = \frac{2}{\eta}\frac{\hat{R}}{\hat{h}}\left(\frac{\hat{\mu}\hat{U}}{\hat{\gamma}}\right)^{1/3}, \tag{2.4}$$

which is assumed to be $O(1)$. The numerical constant $\eta \approx 0.894$ incorporates the Bretherton pressure drops across the advancing and retreating menisci [16,18].

Analytical solutions of the system equations (2.1)–(2.3) have been found for the cases of $N = 1$ and $N = 2$ by Booth *et al.* [17,19], respectively. A general analytical solution is no longer possible for $N \geq 3$; thus, numerical solutions or reduced-order models are required to investigate such systems. Following the methodology of Crowdy [29], one can write down a general solution for an arbitrary number of bubbles in terms of Schottky–Klein prime functions, in which the unknown coefficients satisfy a set of coupled nonlinear integral equations. Alternatively, Booth *et al.* [17] presented a numerical approach based on reformulating equations (2.1) in terms of the streamfunction and solving the resulting system using finite-element methods. Solutions found using this methodology were presented for values of N up to 4, and we use it below to validate the reduced-order models derived in §§3 and 4.

3. Dipole model

3.1. Model set-up

In this section, we consider the motion of N bubbles that are far away from each other and use the method of matched asymptotic expansions to derive a system of $2N$ ordinary differential equations (ODEs) to approximate the behaviour of the full system equations (2.1)–(2.3). The asymptotic structure of our problem is as follows. In the outer problem, the bubbles act like point dipoles, and the inner problem is that of an

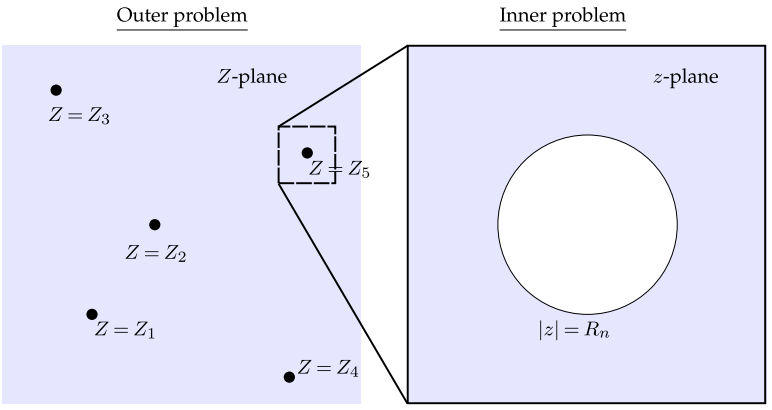

Figure 2. Schematic of the asymptotic structure: (a) the outer problem, in which the points $Z = Z_k$ represent the bubble positions; (b) the inner problem for the nth bubble, in which $|z| = R_n$ is the bubble surface.

isolated bubble that experiences a uniform background flow plus the effect of the other bubbles in the far field. In figure 2, we show the asymptotic structure schematically.

We begin by reformulating equations (2.1) using complex variables. Let $\nu \ll 1$ be the ratio of a typical bubble radius to a typical centre–centre distance. Suppose that the nth bubble, with dimensionless radius R_n, is at position $(x_n, y_n) = (X_n/\nu, Y_n/\nu)$. We then rescale lengths with $1/\nu$, so the rescaled distance between bubbles is $O(1)$ and the bubble radii are $O(\nu)$.

Let $Z = X + \mathrm{i}Y = \nu(x + \mathrm{i}y)$, where (x, y) are the original unscaled variables used in the model equations (2.1), and (X, Y) are the new outer variables. Then we define the complex potential $\mathcal{W}(Z) = \nu\big(-p(X, Y) + \mathrm{i}\psi(X, Y)\big)$, where ψ is the streamfunction. Thus, W is a holomorphic function that satisfies the boundary conditions [30]

$$\mathrm{Im}[\mathcal{W}(Z)] = \nu q_n + \mathrm{Im}\left[\overline{\mathcal{U}}_n(Z - Z_n)\right] \qquad \text{on} \quad |Z - Z_n| = \nu R_n, \tag{3.1a}$$

for each $1 \le n \le N$, and the far-field condition

$$\mathcal{W}(Z) \sim Z + o(1) \qquad \text{as} \quad Z \to \infty, \tag{3.1b}$$

where $\mathcal{U}_n = U_n + \mathrm{i}V_n$ is the complex representation of the nth bubble velocity, the q_n are *a priori* unknown constants and the over-bar denotes complex conjugation.

3.2. Asymptotic expansions

3.2.1. Outer problem

In the outer problem, in the limit $\nu \to 0$, the bubbles shrink to the points $Z = Z_n$ for each $1 \le n \le N$ (see equation (3.1a) and figure 2a). Here, we expand the complex potential as

$$\mathcal{W}(Z) \sim Z + \nu\mathcal{W}_1(Z) + \nu^2\mathcal{W}_2(Z) + \cdots \qquad \text{as} \quad \nu \to 0. \tag{3.2}$$

Note that the leading-order solution is simply the far-field uniform flow and that $\mathcal{W}(Z)$ is holomorphic in $\mathbb{C}$ except at the positions of the bubble centres $Z = Z_n$, for $1 \le n \le N$.

3.2.2. Inner problem

We look at the inner region near the nth bubble by scaling $(Z - Z_n) = \nu z$ and $\mathcal{W}(Z) = \nu w(z)$, where z and $w(z)$ are $O(1)$. The inner problem is that of an isolated bubble of radius R_n centred at the origin (figure 2b). Again, we expand our variables in powers of ν as

$$w(z) \sim w_0(z) + \nu w_1(z) + \nu^2 w_2(z) + \cdots \qquad \text{as} \quad \nu \to 0, \tag{3.3a}$$

$$\mathcal{U}_n \sim \mathcal{U}_n^{(0)} + \nu\mathcal{U}_n^{(1)} + \nu^2\mathcal{U}_n^{(2)} + \cdots \qquad \text{as} \quad \nu \to 0, \tag{3.3b}$$

$$q_n \sim q_n^{(0)} + \nu q_n^{(1)} + \nu^2 q_n^{(2)} + \cdots \qquad \text{as} \quad \nu \to 0. \tag{3.3c}$$

Here, $w(z)$ is a holomorphic function in the region $|z| > R_n$.

3.3. Leading-order inner solution

The leading-order inner complex potential then satisfies the boundary conditions

$$\mathrm{Im}[w_0(z)] = q_n^{(0)} + \mathrm{Im}\left[\overline{\mathcal{U}}_n^{(0)} z\right] \qquad \text{on} \quad |z| = R_n, \tag{3.4a}$$

$$w_0(z) \sim z \qquad \text{as} \quad z \to \infty, \tag{3.4b}$$

which are solved by

$$w_0(z) = z + \frac{\left(1 - \mathcal{U}_n^{(0)}\right) R_n^2}{z}, \tag{3.5}$$

with $q_n^{(0)} = 0$. This solution is equivalent to the pressure field found in [17] for an isolated bubble of radius R_n, as expected in the large-separation limit.

3.4. Correction to the outer solution

The leading-order inner solution equation (3.5) induces a correction to the outer solution at $O(\nu^2)$. Therefore, by Van Dyke's matching rule [31], we find that $\mathcal{W}_1(Z) \equiv 0$ and $\mathcal{W}_2(Z)$ satisfies

$$\mathcal{W}_2(Z) \sim \frac{\left(1 - \mathcal{U}_k^{(0)}\right) R_k^2}{Z - Z_k} \qquad \text{as} \quad Z \to Z_k \tag{3.6}$$

for each $1 \le k \le N$. Since $\mathcal{W}_2(Z) \to 0$ as $Z \to \infty$, we find that

$$\mathcal{W}_2(Z) = \sum_{k=1}^{N} \frac{\left(1 - \mathcal{U}_k^{(0)}\right) R_k^2}{Z - Z_k}. \tag{3.7}$$

3.5. Correction to the inner solution

3.5.1. $O(\nu)$

Using equation (3.7), we find that the $O(\nu)$ correction to the inner solution satisfies the boundary conditions

$$\mathrm{Im}[w_1(z)] = q_n^{(1)} + \mathrm{Im}\left[\overline{\mathcal{U}}_n^{(1)} z\right] \qquad \text{on} \quad |z| = R_n, \tag{3.8a}$$

$$w_1(z) \sim \sum_{\substack{k=1 \\ k \neq n}}^{N} \frac{\left(1 - \mathcal{U}_k^{(0)}\right) R_k^2}{Z_n - Z_k} \qquad \text{as} \quad z \to \infty. \tag{3.8b}$$

This problem is solved by

$$w_1(z) = -\frac{\mathcal{U}_n^{(1)} R_n^2}{z} + \sum_{\substack{k=1 \\ k \neq n}}^{N} \frac{\left(1 - \mathcal{U}_k^{(0)}\right) R_k^2}{Z_n - Z_k} \tag{3.9}$$

and

$$q_n^{(1)} = \mathrm{Im}\left[\sum_{\substack{k=1 \\ k \neq n}}^{N} \frac{\left(1 - \mathcal{U}_k^{(0)}\right) R_k^2}{Z_n - Z_k}\right]. \tag{3.10}$$

When computing the force balance equation (2.3) at the end of this section, we shall find that $\mathcal{U}_n^{(1)} \equiv 0$. Therefore, we must continue to $O(\nu^2)$ to find the first non-zero correction to the bubble velocity.

3.5.2. $O(\nu^2)$

Continuing to the next asymptotic order in the inner problem, we find that $w_2(z)$ satisfies the boundary conditions

$$\mathrm{Im}[w_2(z)] = q_n^{(2)} + \mathrm{Im}\left[\overline{\mathcal{U}}_n^{(2)} z\right] \qquad \text{on} \quad |z| = R_n, \tag{3.11a}$$

$$w_2(z) \sim -\left(\sum_{\substack{k=1\\k\neq n}}^{N} \frac{\left(1-\mathcal{U}_k^{(0)}\right)R_k^2}{(Z_n - Z_k)^2}\right) z \qquad \text{as} \quad z \to \infty, \tag{3.11b}$$

which are solved by

$$w_2(z) = -\left(\sum_{\substack{k=1\\k\neq n}}^{N} \frac{\left(1-\mathcal{U}_k^{(0)}\right)R_k^2}{(Z_n - Z_k)^2}\right) z - \left(\mathcal{U}_n^{(2)} + \sum_{\substack{k=1\\k\neq n}}^{N} \frac{\left(1-\mathcal{U}_k^{(0)}\right)R_k^2}{\overline{(Z_n - Z_k)}^2}\right) \frac{R_n^2}{z} \tag{3.12}$$

and $q_n^{(2)} = 0$.

3.6. Bubble velocity

Now that we have solved for $w(z)$, we perform the effective force balance equation (2.3) on each bubble by evaluating

$$\frac{1}{\mathrm{i}\pi} \oint_{|z|=R_n} w(z)\,\mathrm{d}z = -R_n^2 \mathcal{U}_n + \frac{R_n \mathcal{U}_n}{\delta \left|\mathcal{U}_n\right|^{1/3}}. \tag{3.13}$$

Substituting our expansions equations (3.3) for $w(z)$ and $\mathcal{U}_n$, we find at leading order that the force balance equation (3.13) gives

$$2\left(1-\mathcal{U}_n^{(0)}\right)R_n^2 = -R_n^2 \mathcal{U}_n^{(0)} + \frac{R_n \mathcal{U}_n^{(0)}}{\delta \left|\mathcal{U}_n^{(0)}\right|^{1/3}}, \tag{3.14}$$

which is simply the equation of motion for an isolated bubble of radius R_n [17]. To leading order, each bubble therefore moves as if it were in isolation in a uniform background flow. Thus, $\mathcal{U}_n^{(0)} = U_n^{(0)} \in \mathbb{R}$, and equation (3.14) simplify to

$$\frac{\left(U_n^{(0)}\right)^{2/3}}{2 - U_n^{(0)}} = \delta R_n. \tag{3.15}$$

At $O(\nu)$, we find the force balance equation (3.13) gives

$$-2\mathcal{U}_n^{(1)} = -\mathcal{U}_n^{(1)} + \frac{1}{\delta R_n \left(U_n^{(0)}\right)^{1/3}} \left(\mathcal{U}_n^{(1)} - \frac{1}{3}\,\mathrm{Re}\left[\mathcal{U}_n^{(1)}\right]\right), \tag{3.16}$$

which is solved by $\mathcal{U}_n^{(1)} = 0$. As alluded to in §3.5.1, we need to advance to $O(\nu^2)$ to find the correction to the bubble velocity owing to the presence of the other bubbles.

The force balance at $O(\nu^2)$ is given by

$$-2\left(\mathcal{U}_n^{(2)} + \sum_{\substack{k=1\\k\neq n}}^{N} \frac{\left(1-U_k^{(0)}\right)R_k^2}{\overline{(Z_n - Z_k)}^2}\right) = -\mathcal{U}_n^{(2)} + \frac{1}{\delta R_n \left(U_n^{(0)}\right)^{1/3}} \left(\mathcal{U}_n^{(2)} - \frac{1}{3}\,\mathrm{Re}\left[\mathcal{U}_n^{(2)}\right]\right). \tag{3.17}$$

By writing $\mathcal{U}_n^{(2)} = U_n^{(2)} + \mathrm{i}V_n^{(2)}$ and taking the real and imaginary parts of equation (3.17), we obtain

$$U_n^{(2)} = -\frac{6U_n^{(0)}}{4 + U_n^{(0)}} \operatorname{Re}\left[\sum_{\substack{k=1\\k\neq n}}^{N} \frac{\left(1 - U_k^{(0)}\right) R_k^2}{\overline{(Z_n - Z_k)}^2}\right], \tag{3.18a}$$

$$V_n^{(2)} = -U_n^{(0)} \operatorname{Im}\left[\sum_{\substack{k=1\\k\neq n}}^{N} \frac{\left(1 - U_k^{(0)}\right) R_k^2}{\overline{(Z_n - Z_k)}^2}\right]. \tag{3.18b}$$

3.7. Dipole model

Using the results equations (3.14) and (3.18), we create a dynamical system for the bubble positions $z_n = x_n + \mathrm{i}y_n$ for each $1 \le n \le N$, namely

$$\frac{\mathrm{d}x_n}{\mathrm{d}t} = U_n^{(0)} - \frac{6U_n^{(0)}}{4 + U_n^{(0)}} \sum_{\substack{k=1\\k\neq n}}^{N} \frac{R_k^2 \left(1 - U_k^{(0)}\right)((x_n - x_k)^2 - (y_n - y_k)^2)}{((x_n - x_k)^2 + (y_n - y_k)^2)^2}, \tag{3.19a}$$

$$\frac{\mathrm{d}y_n}{\mathrm{d}t} = -2U_n^{(0)} \sum_{\substack{k=1\\k\neq n}}^{N} \frac{R_k^2 \left(1 - U_k^{(0)}\right)(x_n - x_k)(y_n - y_k)}{((x_n - x_k)^2 + (y_n - y_k)^2)^2}. \tag{3.19b}$$

The first term on the right-hand side of equation (3.19a) represents the leading-order effect of each bubble simply being transported by the background flow, and the series terms in equations (3.19) represent the dipole interactions between the bubbles. Given the value of the parameter δ and the bubble radius R_k, each $U_k^{(0)}$ is determined once and for all by equation (3.15). The system (equations (3.19)) is referred to as the 'dipole model' and provides a set of $2N$ real ODEs that are significantly easier to solve than the full model equations (2.1)–(2.3). These equations are amenable to any standard ODE solver; we use the built-in NDSolve solver in Mathematica [32].

In comparison with dipole models in the literature [20,22,23], our system (equations (3.19)) systematically includes the drag owing to the thin films, resulting in a closed model with no ad hoc fitting parameters. The calculated strength of the dipole interaction in equations (3.19) is anisotropic, with differing contributions parallel and perpendicular to the flow direction (corresponding to equations (3.19a) and (3.19b), respectively). In either case, we calculate precisely how the interaction term depends on the dimensionless parameter δ and on the radius of each bubble, both through the explicit dependence on R_k and through $U_k^{(0)}$, which is determined by equation (3.15).

If the bubbles have different radii R_k, then the corresponding values of $U_k^{(0)}$ are also different, and the dipole dynamics is dominated by the leading term in equation (3.19a). In this case, each bubble is primarily carried along by the background flow, with a velocity that is an increasing function of the bubble radius, and the inter-bubble interactions have a relatively small effect. However, if the bubbles are identical ($R_k \equiv 1$ without loss of generality), then the velocities $U_k^{(0)}$ owing to the background flow are all equal. In this case, the *relative* bubble velocities are entirely due to the interaction terms in equations (3.19). Finally, if $R_k \equiv 1$ and $\delta = 1$, then equation (3.15) gives $U_k^{(0)} = 1$, and we find from equations (3.19) that $\mathcal{U}_n \equiv 1$. In this case, the bubbles all travel at precisely the same velocity as the background flow, reproducing the result for the full model found by [17]. Hence, the dipole model is exact for $\delta = 1$, if the bubbles are all identical.

In the next section, we derive an alternative reduced model based on summing over the interactions between each pair of bubbles.

4. Pairwise interaction model

4.1. Model set-up

Booth *et al.* [19] found the analytical solution of the problem equation (3.1) for $N = 2$ bubbles in a Hele-Shaw cell, which we summarize in appendix B. Here, we use this result to develop a pairwise interaction model for the propagation of an arbitrary number of bubbles.

Suppose we have a system of N bubbles at positions $z_n = x_n + \mathrm{i}y_n$ $(1 \le n \le N)$ in the complex z-plane, with dimensionless radii R_n. We then approximate the full solution of equations (2.1)–(2.3) by considering the interaction between each pair of bubbles. To that end, we choose two bubbles labelled n and k, with $n \neq k$, and then the complex potential $w(z)$ for the flow owing to just these two bubbles satisfies the boundary conditions

$$\mathrm{Im}[w(z)] = Q_n + \mathrm{Im}\left[\overline{\mathcal{U}}_n z\right] \qquad \text{on} \quad |z - z_n| = R_n, \tag{4.1a}$$

$$\mathrm{Im}[w(z)] = Q_k + \mathrm{Im}\left[\overline{\mathcal{U}}_k z\right] \qquad \text{on} \quad |z - z_k| = R_k, \tag{4.1b}$$

$$w(z) \sim z + o(1) \qquad \text{as} \quad z \to \infty, \tag{4.1c}$$

where the Q_k are *a priori* unknown constants. We introduce the scalings $z = R_n\tilde{z}$ and $w(z) = R_n\tilde{w}(\tilde{z})$, which transform equations (4.1) into

$$\mathrm{Im}[\tilde{w}(\tilde{z})] = q_n + \mathrm{Im}\left[\overline{\mathcal{U}}_n \tilde{z}\right] \qquad \text{on} \quad |\tilde{z} - \tilde{z}_n| = 1, \tag{4.2a}$$

$$\mathrm{Im}[\tilde{w}(\tilde{z})] = q_k + \mathrm{Im}\left[\overline{\mathcal{U}}_k \tilde{z}\right] \qquad \text{on} \quad |\tilde{z} - \tilde{z}_k| = R_{kn}, \tag{4.2b}$$

$$\tilde{w}(\tilde{z}) \sim \tilde{z} + o(1) \qquad \text{as} \quad \tilde{z} \to \infty, \tag{4.2c}$$

where $R_{kn} = R_k/R_n$ and $q_j = Q_j/R_n$. The force balance (equation 2.3) can then be written as

$$\oint_{|\tilde{z}-\tilde{z}_n|=1} \tilde{w}(\tilde{z})\,\mathrm{d}\tilde{z} = -\mathcal{U}_n + \frac{\mathcal{U}_n}{\delta R_n |\mathcal{U}_n|^{1/3}}. \tag{4.3}$$

The solution to the two-bubble problem equations (4.2) is presented in appendix B. The centre–centre distance σ_{kn} and corresponding angle ϕ_{kn} are defined such that

$$\tilde{z}_k - \tilde{z}_n = \sigma_{kn} \mathrm{e}^{\mathrm{i}\phi_{kn}}. \tag{4.4}$$

Then the integral on the left-hand side of equation (4.3) can be evaluated in the form [19]

$$\oint_{|\tilde{z}-\tilde{z}_n|=1} \tilde{w}(\tilde{z})\,\mathrm{d}\tilde{z} = -2\,(\mathcal{U}_n - 1) + \mathrm{e}^{2\mathrm{i}\phi_{kn}}\,(\mathcal{U}_k - 1) f_{kn}^{(1)} - (\mathcal{U}_n - 1) f_{kn}^{(2)}, \tag{4.5}$$

where

$$f_{kn}^{(1)}(\sigma_{kn}, R_{kn}) = \frac{2(1 - a_{kn}^2)^2}{a_{kn}^2} \frac{\Psi'_{X_{kn}^2}(1)}{4\log^2 X_{kn}}, \tag{4.6a}$$

$$f_{kn}^{(2)}(\sigma_{kn}, R_{kn}) = \frac{2(1 - a_{kn}^2)^2}{a_{kn}^2} \frac{\Psi'_{X_{kn}^2}\left(\frac{\log a_{kn}}{\log X_{kn}}\right)}{4\log^2 X_{kn}} - 2. \tag{4.6b}$$

Here, Ψ is the q-digamma function [33], the prime $'$ represents differentiation and we define the quantities

$$a_{kn} = \frac{\sigma_{kn}^2 - R_{kn}^2 + 1 - \sqrt{(\sigma_{kn}^2 - R_{kn}^2 + 1)^2 - 4\sigma_{kn}^2}}{2\sigma_{kn}}, \tag{4.7a}$$

$$X_{kn} = a_{kn}^2 + \frac{(R_{kn} - 1)a_{kn}(a_{kn} + 1)(\sigma_{kn} - R_{kn} - 1)}{\sigma_{kn}(\sigma_{kn} - R_{kn} - a_{kn})}. \tag{4.7b}$$

We note that the leading term $-2(\mathcal{U}_n - 1)$ in equation (4.5) is the contribution owing to the external flow and not the influence of the other bubble. It is important not to over-count this contribution when we sum over the pairwise interactions in the next subsection.

4.2. Equations of motion

We now sum the pairwise terms in equation (4.5). For a system of N bubbles, the left-hand side of equation (4.5) is approximated by

$$\oint_{|\tilde{z}-\tilde{z}_n|=1} \tilde{w}(\tilde{z})\,\mathrm{d}\tilde{z} = \sum_{\substack{k=1 \\ k\neq n}}^{N} f_{kn}^{(1)}\,(\mathcal{U}_k - 1)\,\mathrm{e}^{2\mathrm{i}\phi_{kn}} - \left(2 + \sum_{\substack{k=1 \\ k\neq n}}^{N} f_{kn}^{(2)}\right)(\mathcal{U}_n - 1). \tag{4.8}$$

Combining equations (4.3) and (4.8), we obtain the following equations of motion for the pairwise interaction model:

$$\sum_{\substack{k=1\\k\neq n}}^{N} f_{kn}^{(1)}(\mathcal{U}_k-1)\,\mathrm{e}^{2\mathrm{i}\phi_{kn}}-\left(2+\sum_{\substack{k=1\\k\neq n}}^{N} f_{kn}^{(2)}\right)(\mathcal{U}_n-1)=-\mathcal{U}_n+\frac{\mathcal{U}_n}{\delta R_n\left|\mathcal{U}_n\right|^{1/3}}, \tag{4.9}$$

for each $1\le n\le N$. Equation (4.9) gives us N nonlinear algebraic equations for the bubble velocities, a system that is significantly easier to solve than the full problem equations (2.1)–(2.3). However, as we have to solve equation (4.9) at each time step and then evolve the system using $\dot{z}_k=\mathcal{U}_k$, it is slightly more complicated than the dipole method (equations (3.19)). Here, we update the bubble positions using the forward Euler method for simplicity, with a time step of 0.01 (convergence was tested against smaller time steps with a relative error of less than 10^{-5} in the bubble positions).

We next verify that the pairwise interaction model equation (4.9) reduces to the dipole model in the large-separation limit.

4.3. Reduction to the dipole model

In the limit where the distances between bubbles are large (i.e. $\sigma_{kn}/R_{kn}\to\infty$), we find that

$$f_{kn}^{(1)}\sim\frac{2R_{kn}^2}{\sigma_{kn}^2}+O\left(\frac{R_{kn}^5}{\sigma_{kn}^5}\right), \tag{4.10a}$$

$$f_{kn}^{(2)}\sim\frac{2R_{kn}^2}{\sigma_{kn}^4}+O\left(\frac{R_{kn}^5}{\sigma_{kn}^5}\right). \tag{4.10b}$$

We let $\sigma_{kn}=s_{kn}/\nu$, where $s_{kn}=O(1)$ and, as in §3, $\nu\ll1$ measures a typical bubble–bubble distance relative to a typical bubble radius, and expand

$$\mathcal{U}_n\sim\mathcal{U}_n^{(0)}+\nu^2\mathcal{U}_n^{(2)}+\cdots\qquad\text{as}\quad\nu\to0. \tag{4.11}$$

At $O(1)$ in equation (4.9), we find

$$2\left(1-\mathcal{U}_n^{(0)}\right)=-\mathcal{U}_n^{(0)}+\frac{\mathcal{U}_n^{(0)}}{\delta R_n\left|\mathcal{U}_n^{(0)}\right|^{1/3}}, \tag{4.12}$$

which is equivalent to equation (3.14), so we can write $\mathcal{U}_n^{(0)}=U_n^{(0)}\in\mathbb{R}$. Then at $O(\nu^2)$ we find

$$\sum_{\substack{k=1\\k\neq n}}^{N}\frac{2R_{kn}^2}{s_{kn}^2}\left(U_k^{(0)}-1\right)\mathrm{e}^{2\mathrm{i}\phi_{kn}}-2\mathcal{U}_n^{(2)}=-\mathcal{U}_n^{(2)}+\frac{1}{\delta R_n\left(U_n^{(0)}\right)^{1/3}}\left(\mathcal{U}_n^{(2)}-\frac{1}{3}\,\mathrm{Re}\left[\mathcal{U}_n^{(2)}\right]\right), \tag{4.13}$$

which is equivalent to equation (3.17).

Thus, as expected, the pairwise interaction model equation (4.9) reduces to the dipole model equations (3.19) in the dilute limit, where all the bubbles are far apart. However, the pairwise model also correctly describes the interaction when any pair of bubbles becomes so close that the dipole model loses validity. In the next section, we compare the results of both reduced models with numerical solutions of the full problem equations (2.1)–(2.3) for some simple model systems of identical bubbles.

5. Comparison between dipole, pairwise and full numerical solutions

5.1. Three collinear bubbles

In figure 3, we plot three snapshots of the motion of three identical collinear bubbles and show the dimensionless time to reach each configuration, computed by numerical solution of the full system (equations (2.1)–(2.3)) [17], the dipole model equations (3.19) and the pairwise interaction model equation (4.9). Here, $R_1=R_2=R_3=1$ (without loss of generality), $\delta=5$ and the initial bubble separations are set to be 0.04 and 1. We observe that the reduced models predict the same qualitative behaviour as found

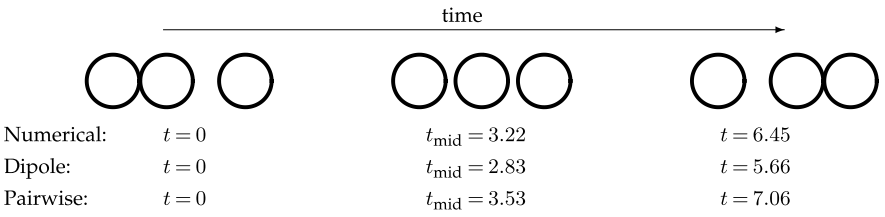

Figure 3. The progression of a series of three identical bubbles with $\delta = 5$ at time points: (i) beginning, (ii) when the bubbles are equidistant and (iii) when the front two bubbles touch, for the numerical solution [17], the dipole model equations (3.19) and the pairwise model equation (4.9). Here, t_{mid} is the value of t at which the bubbles are equally spaced.

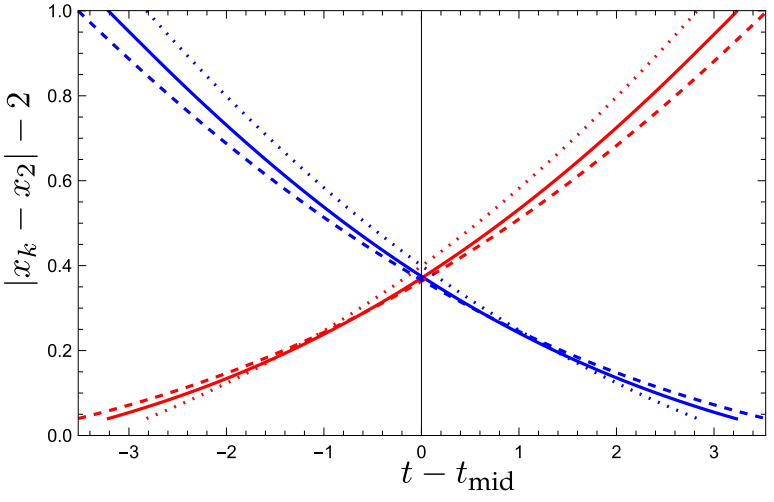

Figure 4. The distance between consecutive bubble edges $|x_k - x_2| - 2$ for $k \in \{1, 3\}$ (red and blue, respectively) versus time, $t - t_{\text{mid}}$, with $\delta = 5$, for the numerical solution (solid), dipole solution equations (3.19) (dotted) and pairwise model equation (4.9) (dashed). Here, t_{mid} is the value of t at which the bubbles are equally spaced for each model.

by the full numerical solution, where the central bubble moves faster than the outer bubbles and so eventually joins with the front-most bubble. However, the dipole model under-predicts the time taken for the exchange, while the pairwise model over-predicts it, by factors of approximately 12.2 and 9.5%, respectively.

In figure 4, we plot the distance between the edges of consecutive bubbles $|x_k - x_2| - 2$ versus $t - t_{\text{mid}}$, where t_{mid} is the time taken for the bubbles to be equally spaced (note that the value of t_{mid} is different for each model). The evident symmetry in the figure confirms that each model retains the reversibility property of Stokes flow. We observe that, although the bubbles are defined to be equidistant at $t = t_{\text{mid}}$, the separations predicted at this point are different for each model, with the pairwise model (dashed) giving a noticeably better approximation to the full model (solid).

In figure 5, we plot the instantaneous velocity, U_2, of the middle bubble in a train of three collinear identical bubbles versus its position, x_2, with $\delta = 5$ and $\delta = 0.25$. We fix the positions of the outer bubbles at $x_1 = -10$ and $x_3 = 2.04$. When $x_2 = -4$, the middle bubble is well separated from the other bubbles (with $x_2 - x_1 = 6$ and $x_3 - x_2 = 6.04$), and the numerical, dipole and pairwise solutions all align, as expected. However, as x_2 increases and the front two bubbles approach each other, the pairwise model (equation (4.9)) matches the numerical solution much more closely than the dipole model (equations (3.19)). The relative error when the bubbles are close ($x_2 = 0$ and $x_3 - x_2 = 0.04$) is approximately 0.28% for $\delta = 5$ and 0.14% for $\delta = 0.25$, for the pairwise solution, versus approximately 0.73% for $\delta = 5$ and 7.5% for $\delta = 0.25$, for the dipole model. Note that these are the errors for the instantaneous velocity and will accumulate as the bubbles travel along the Hele-Shaw cell. The pairwise model thus has a significantly greater accuracy in situations where δ is small and two bubbles become close together, such as in the cascading effect observed in a collinear train of identical bubbles [17,20]. In contrast, when the bubbles are greater than two radii apart ($x_2 < -3$), the three solutions all align, showing that, as long as the bubbles are well separated, the simple dipole method provides an excellent approximation of the full model dynamics.

Following the numerical method presented in [17] and in appendix A, solutions to the full system take on the order of hours to days of central processing unit (CPU) time to solve, depending on the target time

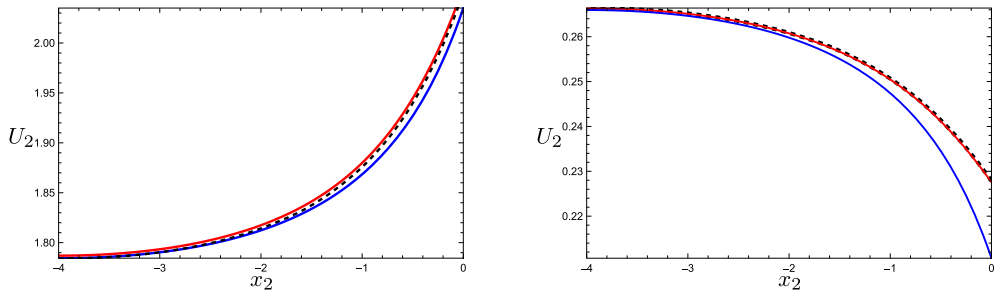

Figure 5. Instantaneous velocity, U_2, of the middle bubble versus its position, x_2, in a system of three collinear identical bubbles with $x_1 = -10, x_3 = 2.04$, and (a) $\delta = 5$ and (b) $\delta = 0.25$. The numerical solution [17] is shown by the black dashed curve, the pairwise interaction model solution equation (4.9) is shown in red and the dipole model solution equations (3.19) is shown in blue.

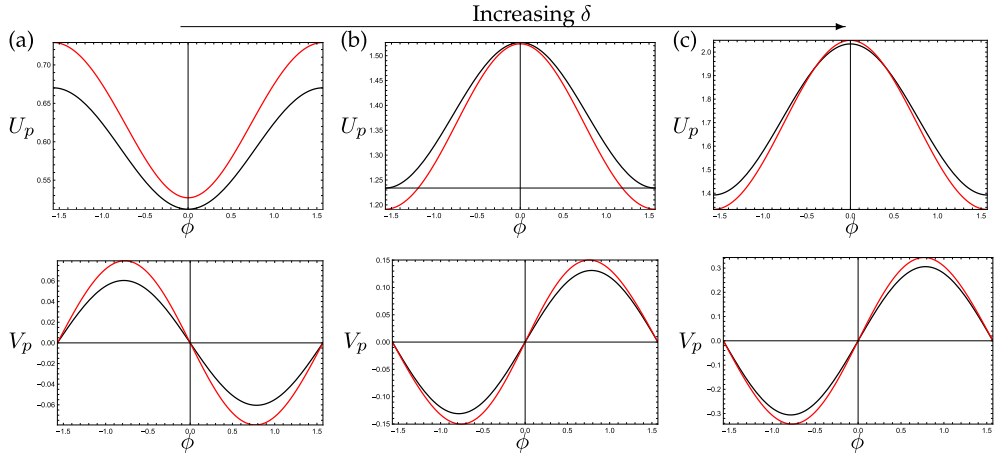

Figure 6. Bubble pair velocity components (U_p, V_p) plotted versus the angle ϕ, for identical touching bubbles with $\delta = 0.5$ (a), 2 (b), 5 (c). The analytical solution (appendix B) is shown in red, and the solution of the dipole model equations (3.19) is shown in black.

and the number of bubbles. In contrast, the ODE methods of the dipole and pairwise models only take a few seconds to run and are readily scaled to large numbers of bubbles and long target times, while still reproducing the dynamics of the full system.

5.2. Pairwise interactions

5.2.1. Touching bubbles

As demonstrated in §5.1, we expect the dipole model to lose accuracy whenever two bubbles are too close. We now consider the 'worst case' scenario of two identical touching bubbles (with $R_1 = R_2 = 1$). In this situation, the pairwise model equation (4.9) is exact: as shown in appendix B, the bubbles move at the same velocity $\mathcal{U}_p = U_p + \mathrm{i}V_p$, and hence the distance between the centres $\sigma = 2$ and angle ϕ between the line joining their centres and the x-axis both remain fixed (figure 14). In figure 6, we plot U_p and V_p versus ϕ for different values of δ. We observe a significant discrepancy between the exact solution and the dipole solution. The maximum discrepancy in the streamwise velocity, U_p, occurs for a perpendicular pair of bubbles ($\phi = \pm\pi/2$), while the error in the transverse velocity, V_p, is maximized when $\phi = \pm\pi/4$.

A pair of touching identical bubbles aligned with ($\phi = 0$) or perpendicular to ($\phi = \pi/2$) the flow travels parallel to the background flow with velocity $U_{||}$ or $U_\perp$, respectively, where each satisfies (appendix B)

$$\frac{U_{||}^{2/3}}{U_{||} + \frac{\pi^2}{6}(1 - U_{||})} = \delta, \qquad \frac{U_\perp^{2/3}}{U_\perp + \frac{\pi^2}{3}(1 - U_\perp)} = \delta. \tag{5.1}$$

In contrast, with $N = 2$, $R_1 = R_2 = 1$, the dipole system (equations (3.19)) simplifies to

$$U_{||} = \frac{U_b(5 + 5U_b)}{2(4 + U_b)}, \qquad U_\perp = \frac{U_b(11 - U_b)}{2(4 + U_b)}, \tag{5.2}$$

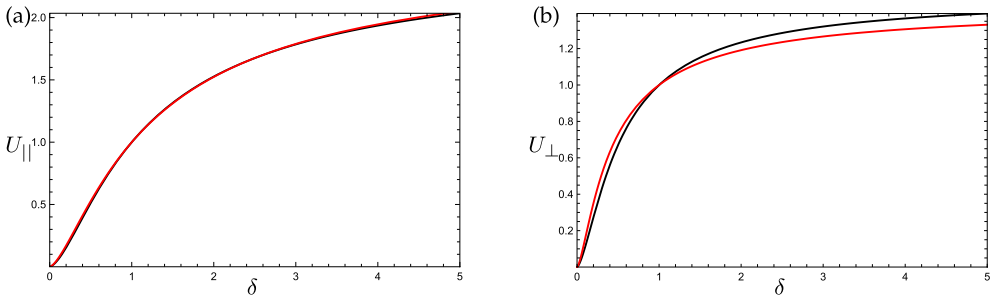

Figure 7. Bubble pair velocity as a function of Bretherton parameter, δ, for two identical touching bubbles (with $N = 2$, $R_1 = R_2 = 1$ and (a) $\phi = 0$, (b) $\phi = \pi/2$). The analytical solution equation (5.1) is shown in red, and the solution of the dipole model equation (5.2) is shown in black.

where U_b is the velocity of an isolated bubble, satisfying equation (3.15) with $R_n = 1$.

In figure 7, we compare the predicted pair velocities equations (5.1) and (5.2) plotted as functions of δ. Although the absolute error is small for $\delta < 1$, the relative error can be large, as indicated in figure 6. Indeed, as $\delta \to 0$, the relative error approaches a constant value $1 - 15\sqrt{3}/\pi^3 \approx 16.2\%$ when $\phi = 0$, and $1 - 33\sqrt{3}/(2\sqrt{2}\pi^3) \approx 35\%$ when $\phi = \pi/2$. In contrast, for $\delta > 1$, the relative error is smaller, but there can be a significant absolute error. In the limit as $\delta \to \infty$, the dipole model equation (5.2) predicts that $U_{||} \to 5/2$ and $U_{\perp} \to 3/2$, while the full model equation (5.1) gives $U_{||} \to \pi^2/(\pi^2 - 6) \approx 2.55$ and $U_{\perp} \to \pi^2/(\pi^2 - 3) \approx 1.44$. This error accumulates as the bubble pair is swept along the Hele-Shaw cell and thus induces significant errors in the positions of the bubbles over time.

We note that the error when the bubbles are aligned with the background flow ($\phi = 0$) is significantly less than when they are perpendicular. This is one explanation as to why the pairwise model only offers a slight improvement over the dipole method for a train of aligned bubbles in §5.1. Finally, we reiterate that the analysis conducted in this section is under worst case conditions for the dipole method. Nevertheless, we find that it still provides a surprisingly good approximation to the full dynamics even when the bubbles are touching and the assumption of large bubble separation certainly does not hold.

5.2.2. Effect of separation

Now we examine in more detail how the accuracy of the dipole model depends on the bubble separation. To illustrate the behaviour, we focus on a particular example of a pair of bubbles, with one twice as large as the other ($R = 2$), and with the line joining their centres making an angle $\phi = \pi/3$ with the flow. In figure 8, we compare the bubble velocities given by the dipole model equations (3.19) and by the analytic solution (given in appendix B), plotted as functions of the centre-to-centre distance σ. We observe that, as expected, the dipole model matches the analytic solution very closely for large σ. However, in the limit $\sigma \to 1 + R$, the dipole approximation fails to accurately capture the strengthening of the interaction effect at close proximity, particularly for small values of δ.

5.3. Bubbles aligned perpendicular to the flow

As demonstrated in §5.2, the dipole method performs least accurately in the situation when the bubbles are aligned perpendicular to the flow direction. In this section, we compare the dipole and pairwise models against the full solution for a system of three identical bubbles initially aligned perpendicular to the background flow direction. The bubbles are initially equally spaced with a dimensionless bubble–bubble separation of 0.1. In this situation, the middle bubble moves horizontally, by symmetry, while the hydrodynamic interactions cause the outer two bubbles to drift apart.

In figure 9a, we plot the trajectory of the centre of the bottom-most bubble with $\delta = 5$ for time $t \in [0, 5]$. Again, we find that both simplified models reproduce the qualitative behaviour of the full model, with the transverse motion being slightly overestimated by the dipole model and underestimated by the pairwise model. In figure 9b, we plot the error in the bubble positions against time, and we observe that the pairwise model offers a small but noticeable improvement in accuracy: at $t = 5$, the errors produced by the dipole and pairwise methods are approximately 0.23 and 0.15, respectively.

The two proposed simplified models allow us to generate long-time solutions of this three-bubble system at minimal computational cost. In figure 10a, we show computed trajectories for the centre of the

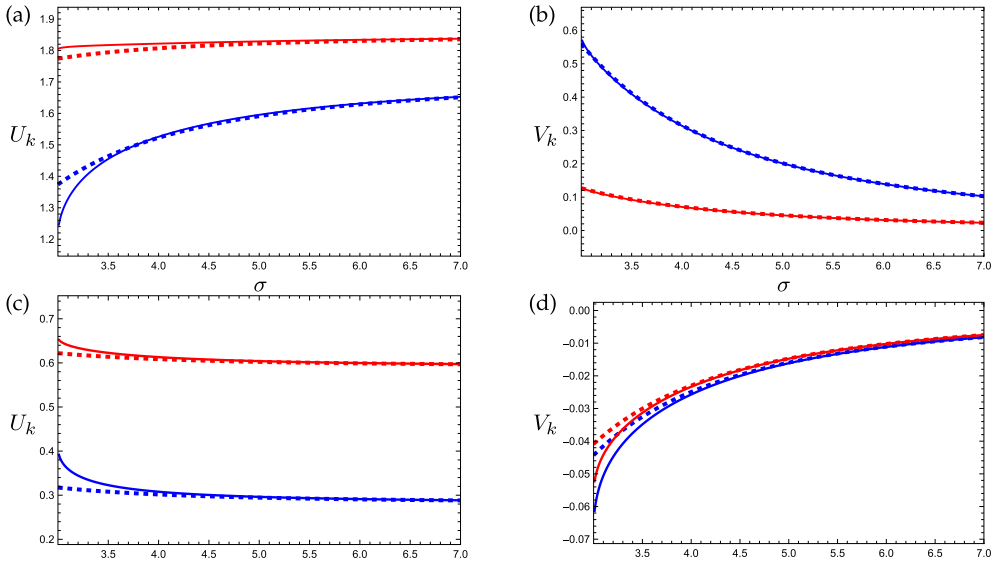

Figure 8. (a and c) Instantaneous bubble velocity in x-direction versus separation, σ, for the smaller bubble U_1 (blue) and the larger bubble U_2 (red), with $R = 2, \phi = \pi/3$ and (a) $\delta = 5$, (c) $\delta = 0.25$. (b and d) Instantaneous bubble velocity in y-direction versus separation, σ, for the smaller bubble V_1 (blue) and the larger bubble V_2 (red), with $R = 2$, $\phi = \pi/3$ and (b) $\delta = 5$, (d) $\delta = 0.25$. The analytic solutions are shown by the solid curves, and the dipole solutions are shown by the dashed curves.

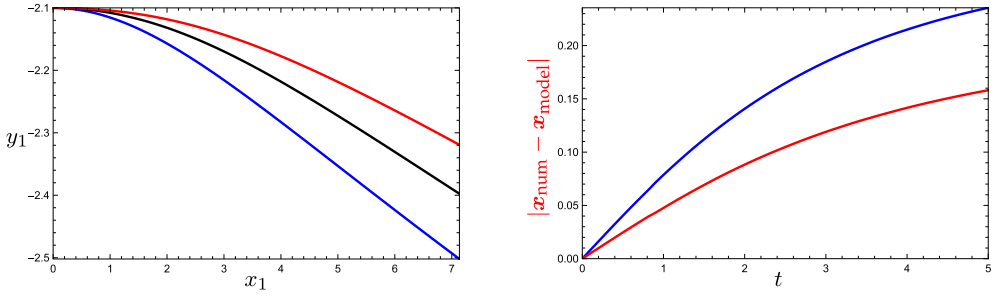

Figure 9. (a) The trajectory (x_1, y_1) of the lowest in a system of three identical bubbles that are initially aligned perpendicular to the background flow with $\delta = 5$ and an initial bubble–bubble separation of 0.1. (b) The error of the dipole (blue) and pairwise (red) models compared with the numerical solution of the full model (black).

lowest bubble extended up to $t = 40$, using both the dipole and the pairwise model. In both cases, the computational cost is on the order of seconds of CPU time, while the full model would require hundreds of CPU hours for the same long-time solutions. In figure 10b, we observe that both methods produce the same qualitative behaviour: the outer bubbles travel faster than the middle one in the x-direction and move away from the middle bubble in the y-direction, fanning the bubbles out into a U-shape (for $\delta < 1$ the outermost bubbles travel slower and the U-shape forms in the opposite direction). Once the bubbles have become sufficiently well separated, the computed velocities using the two models are virtually identical, as expected. However, the early-time discrepancies seen in figure 9 are propagated by the system, leading to persistent errors in the bubble positions at large times.

With the simplified models, it is also simple to include additional bubbles. In figure 11, we plot the configuration at $t = 100$ of nine bubbles initially aligned perpendicular to the flow. We observe similar behaviour to that in the three-bubble case, with the outermost bubbles travelling faster in the x-direction and spreading the bubbles out into a U-shape. The dipole and pairwise models produce the same qualitative behaviour and allow for quick and easy predictions for the dynamics of the bubbles over long times, something that is very much more expensive to obtain by solving the full model.

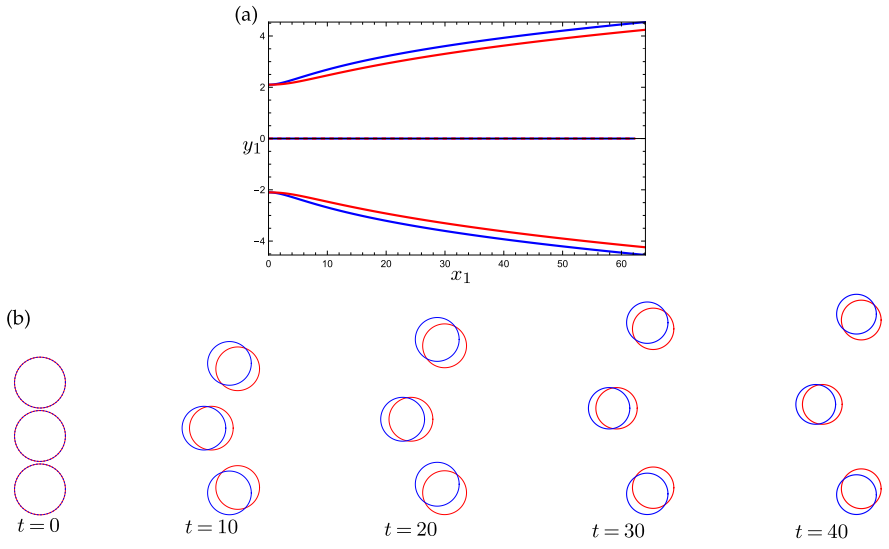

Figure 10. (a) The continuations of the trajectories of three initially perpendicularly aligned bubbles from figure 9, computed using the dipole (blue) and pairwise (red) models for $0 \leq t \leq 40$. (b) Snapshots of the bubble positions at $t = 0,\ 10\ ,\ 20\ ,\ 30\ ,\ 40$ using the dipole (blue) and pairwise (red) models.

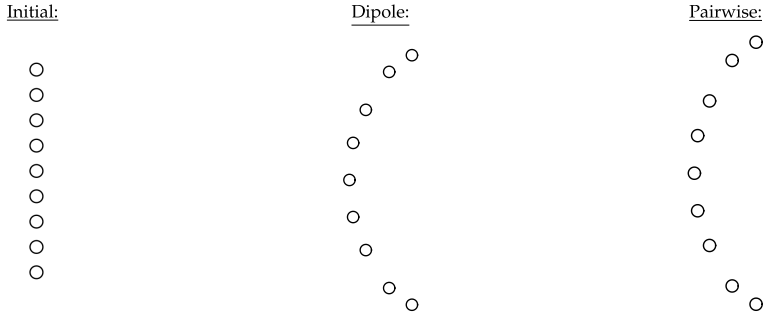

Figure 11. The configuration of nine bubbles at $t = 100$, which were initially all aligned perpendicular to the background flow direction.

6. Conclusions

In this paper, we derive two reduced-order models for the motion of an arbitrary number N of approximately circular bubbles in a Hele-Shaw cell. The first is the so-called dipole model, in which the effect of each bubble on the flow is approximated by a dipole acting at its centre. For the second 'pairwise model', we find approximate equations of motion by summing the interaction terms generated between each pair of bubbles. Each reduced model comprises a system of $2N$ nonlinear ODEs, the solution of which can be found at a much-reduced computational cost compared with the full numerical solution.

Dipole methods are commonly used in the literature to simulate the dynamics of multiple approximately circular bubbles in a Hele-Shaw cell [20,22]. We systematically derive a dipole model using matched asymptotic expansions in the limit where the bubbles are all far apart. As well as providing a theoretical underpinning, this approach allows us to incorporate the Bretherton drag law, rather than the ad hoc linear drag laws often used in the literature [21–24].

Nevertheless, it must be acknowledged that the assumptions underlying the derivation of the dipole model fail when any two bubbles become sufficiently close, and the pairwise model aims to extend the range of validity to cover such cases. While the dipole model is exact for the motion of an isolated bubble ($N = 1$), the pairwise interaction model is exact for the motion of a pair of bubbles ($N = 2$). We demonstrate that the pairwise and dipole models are equivalent when the dipole model is valid, i.e. when the bubbles are all well separated. However, the pairwise model also correctly captures the local interactions between any pair of bubbles that become sufficiently close for the dipole model to break down.

We compare both of the reduced models against each other and against numerical solutions of the full problem for several test cases. We show that they both qualitatively reproduce the Newton's cradle-like behaviour reported by [17], where the middle bubble in a train of three identical collinear bubbles moves

faster or slower than the outer two, depending on whether the Bretherton parameter δ is greater or less than 1. We examine the limiting case of two touching bubbles, for which the pairwise model provides exact solutions, and find that the dipole model can perform surprisingly well even in this worst case situation, especially at larger values of δ. Finally, for a system of three or more bubbles initially aligned perpendicular to the flow direction, we demonstrate an interesting hydrodynamic phenomenon: that the outermost bubbles drift apart and travel ahead of the innermost bubbles (for $\delta > 1$) to form a U-shape. Both of the reduced-order models capture the correct qualitative behaviour and allow us to evolve large systems of bubbles over long time scales that would be extremely computationally costly to access with the full model.

In all of the test cases considered, the dipole model performs well, while the pairwise model provides a small but noticeable improvement in accuracy in situations where two bubbles are close or touching (see figures 5 and 9 and appendix C). In the framework of matched asymptotic expansions, the dipole model is valid for large bubble separation, and, in principle, one should switch to a modified inner problem when any two bubbles become too close. The pairwise model removes the need to check the inter-bubble distance at each time step, since it is equivalent to the dipole model at large separations but correctly describes the pairwise interaction between any two bubbles in close proximity. Of course, the pairwise model itself loses asymptotic validity if any three or more bubbles become too close. Although such a configuration should be very rare in an initially dilute system, a possible next level of sophistication would aim to accurately capture all three-bubble interactions.

In summary, the two reduced-order models presented in this paper provide a framework that can be used to study an arbitrary configuration of bubbles in a Hele-Shaw cell over a long time scale, at a high accuracy and a low computational cost.

Ethics. This work did not require ethical approval from a human subject or animal welfare committee.

Data accessibility. The code used to generate the figures in this paper is included in the electronic supplementary material [34].

Declaration of AI use. We have not used AI-assisted technologies in creating this article.

Authors' contributions. D.J.B.: conceptualization, formal analysis, investigation, software, writing—original draft; I.G.: conceptualization, investigation, writing—review and editing; P.H.: conceptualization, investigation, writing—review and editing.

All authors gave final approval for publication and agreed to be held accountable for the work performed therein.

Conflict of interest declaration. We declare we have no competing interests.

Funding. D.J.B. is grateful to EPSRC, grant reference number EP/V520202/1, for funding and is now funded as part of the Leverhulme Trust Leadership Award 'Shape-Transforming Active Microfluidics' (RL-2019-014) to Tom Montenegro-Johnson at the University of Warwick.

Appendix A. Numerical solutions

A.1. Numerical method

To facilitate the numerical solution, we reformulate the problem equations (2.1)–(2.3) in terms of the streamfunction, ψ, on a truncated solution domain $(x, y) \in [X_{\min}, X_{\max}] \times [-W, W]$. Then ψ satisfies the Dirichlet boundary-value problem

$$\nabla^2 \psi = 0 \qquad \text{in} \quad \Omega, \tag{A 1a}$$

$$\psi(x, y) = \pm W \qquad \text{on} \quad y = \pm W, \tag{A 1b}$$

$$\psi(x, y) = q_k + U_k(y - y_k) - V_k(x - x_k) \qquad \text{on} \quad \partial\Omega_k, \tag{A 1c}$$

$$\psi(x, y) = y \qquad \text{on} \quad x = X_{\min},\, X_{\max}. \tag{A 1d}$$

The boundary condition equation (A 1c) is applied at each of the N bubble surfaces $\partial\Omega_k$, for $k \in \{1, \ldots, N\}$, and the q_k are *a priori* unknown constants, which are found by enforcing the single-valuedness of the pressure, p, by imposing

$$\oint_{\partial\Omega_k} \frac{\partial \psi}{\partial n}\, \mathrm{d}s = 0 \tag{A 2}$$

on each bubble surface. We denote the centroid of each bubble by (x_k, y_k), so $(U_k, V_k) = (\dot{x}_k, \dot{y}_k)$ where the dot represents the time derivative.

The force balances on each bubble equation (2.3), through the use of integration by parts and the Cauchy–Riemann equations, become

$$-\frac{\delta}{\pi}\oint_{\partial\Omega_k}(x-x_k)\frac{\partial\psi}{\partial x}+(y-y_k)\frac{\partial\psi}{\partial y}\,\mathrm{d}x=\frac{R_k^2U_k}{(U_k^2+V_k^2)^{1/6}}, \tag{A 3a}$$

$$-\frac{\delta}{\pi}\oint_{\partial\Omega_k}(x-x_k)\frac{\partial\psi}{\partial x}+(y-y_k)\frac{\partial\psi}{\partial y}\,\mathrm{d}y=\frac{R_k^2V_k}{(U_k^2+V_k^2)^{1/6}}. \tag{A 3b}$$

We decompose the streamfunction as

$$\psi=\psi^{(0)}+\sum_{k=1}^{N}\left(U_k\psi_k^{(1)}+q_k\psi_k^{(2)}-V_k\psi_k^{(3)}\right), \tag{A 4}$$

where $\psi^{(0)}$ satisfies the boundary-value problem

$$\nabla^2\psi^{(0)}=0 \qquad \text{in} \quad \Omega, \tag{A 5a}$$

$$\psi^{(0)}=\pm W \qquad \text{on} \quad y=\pm W, \tag{A 5b}$$

$$\psi^{(0)}=0 \qquad \text{on each} \quad \partial\Omega_k, \tag{A 5c}$$

$$\psi^{(0)}=y \qquad \text{on} \quad x=X_{\min},\, X_{\max}, \tag{A 5d}$$

and each $\psi_k^{(l)}$ satisfies a boundary-value problem that is independent of U_k, V_k and q_k, given by

$$\nabla^2\psi_k^{(l)}=0 \qquad \text{in} \quad \Omega, \tag{A 6a}$$

$$\psi_k^{(l)}=0 \qquad \text{on} \quad y=\pm W, \tag{A 6b}$$

$$\psi_k^{(l)}=\{y,1,x\} \qquad \text{on} \quad \partial\Omega_k, \tag{A 6c}$$

$$\psi_k^{(l)}=0 \qquad \text{on} \quad \partial\Omega_j, \text{ for } j\neq k, \tag{A 6d}$$

$$\psi_k^{(l)}=0 \qquad \text{on} \quad x=X_{\min},\, X_{\max}, \tag{A 6e}$$

where $l\in\{1,2,3\}$ corresponds to the position of the element chosen in equation (A 6c).

The numerical solutions for $\psi^{(0)}$ and $\psi_k^{(l)}$, for $(l,k)\in\{1,2,3\}\times\{1,\ldots,N\}$, are computed using the finite-element routine NDSolve in Mathematica [32]. In all simulations, we truncate the solution domain using $X_{\min}=x_{\min}-20R_{\max}$ and $X_{\max}=x_{\max}+20R_{\max}$, and either $W=20$ or $W=40$, where $x_{\min,\max}$ are the minimum and maximum values of x_k, respectively, and $R_{\max}$ is the maximum value of R_k. Once we have found $\psi^{(0)}$ and $\psi_k^{(l)}$, for $(l,k)\in\{1,2,3\}\times\{1,\ldots,N\}$, we use equations (A 3) to find U_k, V_k and q_k, for each $k\in\{1,\ldots,N\}$. The positions of the bubbles are then evolved using $\dot{x}_k=U_k$ and $\dot{y}_k=V_k$.

We now validate the numerical method against the known two-bubble solution found in appendix B.

A.2. Validation of numerical method

We now compare the exact two-bubble solution with the numerical solution following the approach set out in equations (A 3)–(A 6). We translate the two-bubble problem into our numerical framework by setting $R_1=1$ and $(x_1,y_1)=(0,0)$, and $R_2=R$ and $(x_2,y_2)=(\sigma\cos\phi,\sigma\sin\phi)$. We then examine the effect of varying the truncated width of the solution domain between $W=20$ and $W=40$.

In figure 12, we plot the bubble velocities (U_k,V_k) versus angle ϕ with $R=2$, $\sigma=4$ and $\delta=5$. We observe good agreement between the numerical solutions of equations (A 3)–(A 6) and the analytical solution. The numerical solution with $W=20$ (blue curves) closely follows the behaviour of the full solution but always under-predicts the bubble velocities in the x-direction, U_k. In contrast, when $W=40$, the numerical solution precisely matches the full solution. In figure 13, we plot the bubble velocities (U_k,V_k) versus separation σ with $R=2$, $\phi=\pi/3$, $W=40$ and $\delta=5$. Again, we observe excellent agreement between the numerical solution and the full solution, provided the truncated solution domain size is large enough.

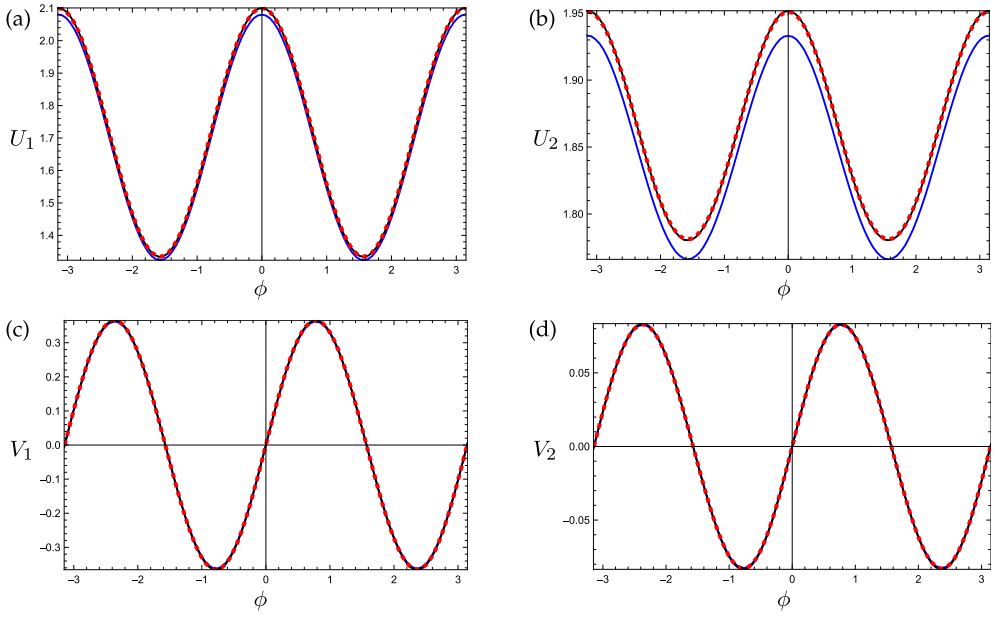

Figure 12. Instantaneous bubble velocity versus angle ϕ for a system of two bubbles with $R = 2$, $\sigma = 4$ and $\delta = 5$. (a, c) The smaller bubble velocity components (U_1, V_1); (b, d) the larger bubble velocity components (U_2, V_2). The analytical solution is shown by the red dashed curve, and the numerical solution is shown in blue for $W = 20$ and black for $W = 40$.

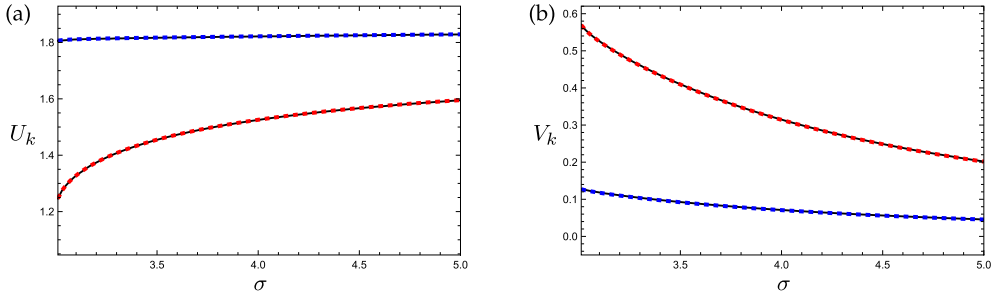

Figure 13. Instantaneous bubble velocity (U_k, V_k) (shown in (a) and (b), respectively) versus separation, σ, for the smaller bubble $k = 1$ (red) and the larger bubble $k = 2$ (blue), with $R = 2$, $\phi = \pi/3$, $\delta = 5$ and $W = 40$. The numerical solution is shown by the black curves, and the analytical solution is shown by the dashed curves.

Appendix B. Summary of the two-bubble solution

Booth *et al.* [19] derive analytical equations of motion for two circular bubbles in a Hele-Shaw cell. We summarize their findings here. Suppose we have two bubbles at positions $z_1 = x_1 + \mathrm{i}y_1$ and $z_2 = x_2 + \mathrm{i}y_2$ in the Argand plane, with dimensionless radii 1 and R, respectively. The bubbles are subject to a uniform background flow of dimensionless magnitude 1 in the positive x-direction. Define the length σ and argument ϕ of the vector joining the centres of the two bubbles, such that $z_2 - z_1 = \sigma \mathrm{e}^{\mathrm{i}\phi}$, as shown schematically in figure 14. The problem is then instantaneously characterized by the values of σ, ϕ and R.

Since the flow is governed by Laplace's equation, we can formulate the problem in terms of the complex potential $w(z) = -p + \mathrm{i}\psi$, where ψ is the streamfunction, and $z = x + \mathrm{i}y$. Then $w(z)$ is holomorphic in the region Ω outside the two bubbles and satisfies the boundary conditions

$$\mathrm{Im}[w(z)] = Q_1 + \mathrm{Im}\left[\overline{\mathcal{U}}_1 z\right] \qquad \text{on} \quad |z - z_1| = 1, \tag{B 1a}$$

$$\mathrm{Im}[w(z)] = Q_2 + \mathrm{Im}\left[\overline{\mathcal{U}}_2 z\right] \qquad \text{on} \quad |z - z_2| = R, \tag{B 1b}$$

$$w(z) \sim z + o(1) \qquad \text{as} \quad z \to \infty, \tag{B 1c}$$

where, for $k \in \{1, 2\}$, we denote by $\mathcal{U}_k = U_k + \mathrm{i}V_k$ the complex representations of the kth bubble velocity, and the Q_k are *a priori* unknown constants.

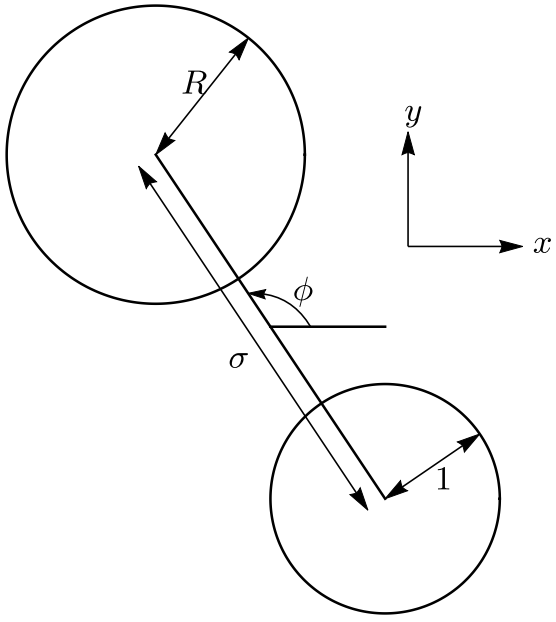

Figure 14. Schematic of the two-bubble problem.

Booth *et al.* [19] use conformal mapping to solve for $w(z)$ and then evaluate equation (2.3) to derive the equations of motion

$$f_1(\sigma,R)(\overline{\mathcal{U}}_2-1)\mathrm{e}^{2\mathrm{i}\phi}-f_2(\sigma,R)(\mathcal{U}_1-1)=-\mathcal{U}_1+\frac{\mathcal{U}_1}{\delta\left|\mathcal{U}_1\right|^{1/3}}, \tag{B 2a}$$

$$f_1(\sigma,R)(\overline{\mathcal{U}}_1-1)\mathrm{e}^{2\mathrm{i}\phi}-f_3(\sigma,R)(\mathcal{U}_2-1)=-R^2\mathcal{U}_2+\frac{R\mathcal{U}_2}{\delta\left|\mathcal{U}_2\right|^{1/3}}, \tag{B 2b}$$

where

$$f_1(\sigma,R)=\frac{(1-a^2)^2}{2a^2\log^2 X}\,\Psi'_{X^2}(1), \tag{B 3a}$$

$$f_2(\sigma,R)=\frac{(1-a^2)^2}{2a^2\log^2 X}\,\Psi'_{X^2}\left(\frac{\log a}{\log X}\right), \tag{B 3b}$$

$$f_3(\sigma,R)=\frac{(1-a^2)^2}{2a^2\log^2 X}\,\Psi'_{X^2}\left(\frac{\log(X/a)}{\log X}\right). \tag{B 3c}$$

Here, Ψ is the q-digamma function [33], and we define the quantities

$$a=\frac{\sigma^2-R^2+1-\sqrt{(\sigma^2-R^2+1)^2-4\sigma^2}}{2\sigma}, \tag{B 4a}$$

$$X=a^2+\frac{(R-1)a(a+1)(\sigma-R-1)}{\sigma(\sigma-R-a)}. \tag{B 4b}$$

The problem simplifies somewhat if the bubbles are identical, in which case we have $R=1$ and

$$f_1(\sigma,1)=\frac{(1-a^2)^2}{8a^2\log^2 a}\,\Psi'_{a^4}(1), \tag{B 5a}$$

$$f_2(\sigma,1)=f_3(\sigma,1)=\frac{(1-a^2)^2}{8a^2\log^2 a}\,\Psi'_{a^4}(1/2), \tag{B 5b}$$

where $a\in(0,1)$ and $\sigma=a+1/a$. Since $f_2=f_3$ in this case, the two equations (B 2) are identical, and it follows that the bubble velocities are equal. The bubble pair velocity $\mathcal{U}_1=\mathcal{U}_2=\mathcal{U}_p$ (say) satisfies

$$f_1(\sigma,1)(\overline{\mathcal{U}}_p-1)\mathrm{e}^{2\mathrm{i}\phi}-f_2(\sigma,1)(\mathcal{U}_p-1)=-\mathcal{U}_p+\frac{\mathcal{U}_p}{\delta\left|\mathcal{U}_p\right|^{1/3}}. \tag{B 6}$$

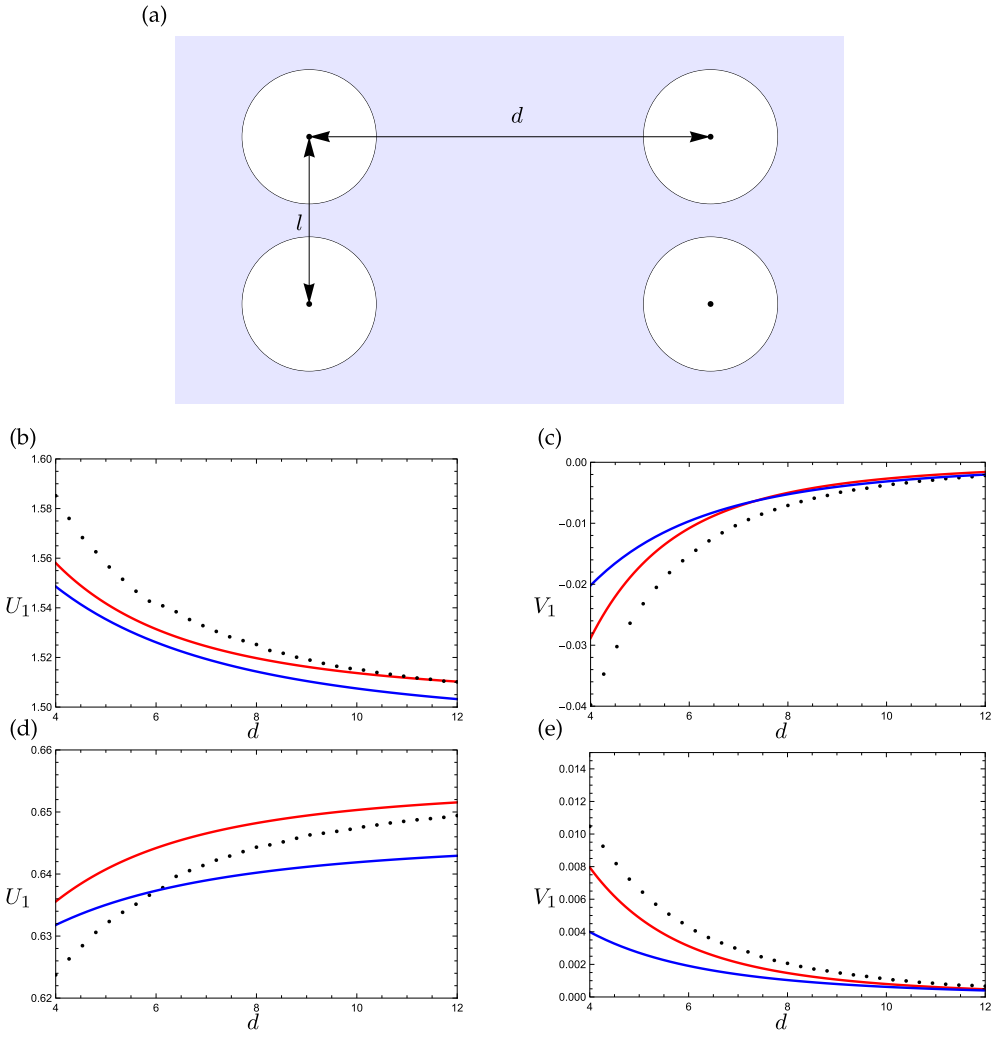

Figure 15. (a) Schematic of four bubbles arranged at the vertices of a rectangle aligned in the flow direction. (b and d) Instantaneous velocity in the *x*-direction of the upper real bubble, U_1, versus centre–centre separation, d, with $l = 2.4$ and (b) $\delta = 5$, (d) $\delta = 0.5$. (c and e) Instantaneous velocity in the *y*-direction of the upper real bubble, V_1, versus centre–centre separation, d, with $l = 2.4$ and (c) $\delta = 5$, (e) $\delta = 0.5$. The numerical solution is shown by the black points, the dipole method equations (3.19) by the blue curves and the pairwise interaction model equation (4.9) by the red curves.

Finally, in the limiting case where the two identical bubbles touch, we have $\sigma \searrow 2$, corresponding to $a \nearrow 1$. By carefully taking the limit in equations (B 5), one finds that

$$f_1(2,1) = \frac{\pi^2}{12}, \qquad f_2(2,1) = f_3(2,1) = \frac{\pi^2}{4}. \tag{B 7}$$

Appendix C. Four bubbles in a rectangle

In this appendix, we consider a configuration of four bubbles that are instantaneously arranged at the vertices of a rectangle (figure 15a). In figure 15b–e, we plot the velocity of the upper rear bubble versus the width of the rectangle, d, for $\delta = 5$ and $\delta = 0.5$, and a fixed rectangle height of $l = 2.4$. Again, we find that the reduced-order models reproduce the qualitative behaviour shown by the full model. Neither reduced model fully captures the nonlinear interaction between all four bubbles when d is small. However, because the pairwise model accurately describes the interactions between each isolated pair of bubbles, it offers an improvement over the dipole model and converges more robustly to the full numerical solution as the distance between the two pairs of bubbles is increased.

References

1. Taylor G, Saffman PG. 1959 A note on the motion of bubbles in a Hele-Shaw cell and porous medium. *Q. J. Mech. Appl. Math*. **12**, 265–279. (doi:10.1093/qjmam/12.3.265)
2. Saffman PG. 1959 Exact solutions for the growth of fingers from a flat interface between two fluids in a porous medium or hele-shaw cell. *Q. J. Mech. Appl. Math* **12**, 146–150. (doi:10.1093/qjmam/12.2.146)
3. Tanveer S. 1986 The effect of surface tension on the shape of a Hele–Shaw cell bubble. *Phys. Fluids* **29**, 3537–3548. (doi:10.1063/1.865831)
4. Maxworthy T. 1986 Bubble formation, motion and interaction in a Hele-Shaw cell. *J. Fluid Mech*. **173**, 95–114. (doi:10.1017/S002211208600109X)
5. Acheson D. 1990 *Elementary fluid dynamics*. Oxford, UK: Oxford University Press.
6. Howison SD. 1986 Fingering in Hele-Shaw cells. *J. Fluid Mech*. **167**, 439–453. (doi:10.1017/S0022112086002902)
7. Howison SD. 1992 Complex variable methods in Hele–Shaw moving boundary problems. *Eur. J. Appl. Math*. **3**, 209–224. (doi:10.1017/S0956792500000802)
8. Cummings LJ, Howison SD, King JR. 1999 Two-dimensional Stokes and Hele-Shaw flows with free surfaces. *Eur. J. Appl. Math*. **10**, 635–680. (doi:10.1017/S0956792599003964)
9. Gustafsson B, Vasil'ev A. 2006 *Conformal and potential analysis in hele-shaw cells*. Berlin, Germany: Springer Science & Business Media.
10. Anna S. 2016 Droplets and bubbles in microfluidic devices. *Annu. Rev. Fluid Mech*. **48**, 285–309. (doi:10.1146/annurev-fluid-122414-034425)
11. Gnyawali V, Moon BU, Kieda J, Karshafian R, Kolios MC, Tsai SSH. 2017 Honey, I shrunk the bubbles: microfluidic vacuum shrinkage of lipid-stabilized microbubbles. *Soft Matter*. **13**, 4011–4016. (doi:10.1039/C7SM00128B)
12. Prakash M, Gershenfeld N. 2007 Microfluidic bubble logic. *Science* **315**, 832–835. (doi:10.1126/science.1136907)
13. Garstecki P, Gitlin I, DiLuzio W, Whitesides GM, Kumacheva E, Stone HA. 2004 Formation of monodisperse bubbles in a microfluidic flow-focusing device. *Appl. Phys. Lett*. **85**, 2649–2651. (doi:10.1063/1.1796526)
14. Zhu L, Gallaire F. 2016 A pancake droplet translating in a Hele-Shaw cell: lubrication film and flow field. *J. Fluid Mech*. **798**, 955–969. (doi:10.1017/jfm.2016.357)
15. Reichert B, Huerre A, Theodoly O, Valignat MP, Cantat I, Jullien MC. 2018 Topography of the lubrication film under a pancake droplet travelling in a Hele-Shaw cell. *J. Fluid Mech*. **850**, 708–732. (doi:10.1017/jfm.2018.457)
16. Wu K, Booth DJ, Griffiths IM, Howell PD, Nunes JK, Stone HA. 2024 Motion and deformation of a bubble in a Hele-Shaw cell. *Phys. Rev. Fluids* **9**, 123603. (doi:10.1103/PhysRevFluids.9.123603)
17. Booth DJ, Griffiths IM, Howell PD. 2023 Circular bubbles in a Hele-Shaw channel: a Hele-Shaw Newton's cradle. *J. Fluid Mech*. **954**, A21. (doi:10.1017/jfm.2022.1008)
18. Bretherton FP. 1961 The motion of long bubbles in tubes. *J. Fluid Mech*. **10**, 166–188. (doi:10.1017/S0022112061000160)
19. Booth D, Wu K, Griffiths I, Howell P, Nunes J, Stone H. 2025 Bubble racing in a Hele-Shaw cell. *J. Fluid Mech*.**1010**, A19.
20. Beatus T, Tlusty T, Bar-Ziv R. 2006 Phonons in a one-dimensional microfluidic crystal. *Nat. Phys*. **2**, 743–748. (doi:10.1038/nphys432)
21. Beatus T, Bar-Ziv RH, Tlusty T. 2012 The physics of 2D microfluidic droplet ensembles. *Phys. Rep*. **516**, 103–145. (doi:10.1016/j.physrep.2012.02.003)
22. Shen B, Leman M, Reyssat M, Tabeling P. 2014 Dynamics of a small number of droplets in microfluidic Hele–Shaw cells. *Exp. Fluids* **55**, 1–10. (doi:10.1007/s00348-014-1728-2)
23. Green Y. 2018 Approximate solutions to droplet dynamics in Hele-Shaw flows. *J. Fluid Mech*. **853**, 253–270. (doi:10.1017/jfm.2018.575)
24. Sarig I, Starosvetsky Y, Gat AD. 2016 Interaction forces between microfluidic droplets in a Hele-Shaw cell. *J. Fluid Mech*. **800**, 264–277. (doi:10.1017/jfm.2016.403)
25. Pumir A, Aref H. 1988 A model of bubble dynamics in a Hele–Shaw cell. *Phys. Fluids* **31**, 752–763. (doi:10.1063/1.866811)
26. Ockendon H, Ockendon J. 1995 *Viscous flow*. vol. 13. Cambridge, UK: Cambridge University Press.
27. Peng GG, Pihler-Puzović D, Juel A, Heil M, Lister JR. 2015 Displacement flows under elastic membranes. Part 2. Analysis of interfacial effects. *J. Fluid Mech*. **784**, 512–547. (doi:10.1017/jfm.2015.589)
28. Burgess D, Foster MR. 1990 Analysis of the boundary conditions for a Hele–Shaw bubble. Phys. Fluids A **2**, 1105–1117. (doi:10.1063/1.857610)
29. Crowdy D. 2008 Explicit solution for the potential flow due to an assembly of stirrers in an inviscid fluid. *J. Eng. Math*. **62**, 333–344. (doi:10.1007/s10665-008-9222-6)
30. Booth D, Griffiths I, Howell P. 2025 The motion of a bubble in a non-uniform hele-shaw flow. *Proc. Roy. Soc. A* **481**, 20240613.
31. Van Dyke M. 1975 Perturbation methods in fluid mechanics. *NASA STI/Recon. Tech. Rep. A* **75**, 46926.
32. Wolfram Research I. 2024 Mathematica, Version 13.0. Champaign, IL: Wolfram Research, Inc.
33. Salem A. 2012 A completely monotonic function involving q-gamma and q-digamma functions. *J. Approx. Theory* **164**, 971–980. (doi:10.1016/j.jat.2012.03.014)
34. Booth DJ, Griffiths I, Howell P. 2026 Supplementary material from: Dipole and pairwise models for the motion of bubbles in a Hele-Shaw cell. Figshare. (doi:10.6084/m9.figshare.c.8311165)